IEEE Access
Multidisciplinary | Rapid Review | Open Access Journal

Received 1 March 2023, accepted 26 March 2023, date of publication 3 April 2023, date of current version 6 April 2023.

Digital Object Identifier 10.1109/ACCESS.2023.3263815

RESEARCH ARTICLE

Direct Voltage MTPA Speed Control of IPMSM-Based Electric Vehicles

MOHAMAD ALZAYED[1], (Member, IEEE), AND HICHAM CHAOUI[1,2], (Senior Member, IEEE)
[1]Intelligent Robotic and Energy Systems Research Group (IRES), Department of Electronics, Carleton University, Ottawa, ON K1S 5B6, Canada
[2]Department of Electrical and Computer Engineering, Texas Tech University, Lubbock, TX 79409, USA

Corresponding author: Mohamad Alzayed (mohamad.alzayed@carleton.ca)

This work was supported by the Natural Sciences and Engineering Research Council of Canada under Grant 315082.

ABSTRACT A simple maximum torque per ampere (MTPA) method is designed for interior permanent magnet synchronous motors (IPMSMs) with no current control. The proposed method tracks the rotor speed by finding the best pair of voltage angle and amplitude for each motor's speed and torque condition. This is achieved without stand for any current control loop and using a single controller, which makes the technology simple to a great extent, contrary to the majority of methodologies in the literature. Moreover, a thorough insight analysis is provided to determine analytically the control gains, which simplifies control and tuning and makes it a suitable contender for the development of low-cost PMSM drives. To illustrate the capability of the suggested control method, a comparative study is conducted using the popular MTPA vector control strategy. Experimental results for various situations reveal the ability of the suggested MTPA controller in steady-state, standstill, and transient conditions. Additionally, to quantitatively assess the MTPA trajectory tracking accuracy, both control methods are compared using an efficiency metric. Besides, the US06 standard driving cycle is implemented experimentally to validate the proposed method for electric vehicle applications.

INDEX TERMS Speed trajectory control, maximum torque per ampere (MTPA), interior PM synchronous motors (IPMSMs).

I. INTRODUCTION

Interior permanent magnet synchronous motors (IPMSMs) have been extensively used thanks to their wide speed operating range and high power density [1], [2], [3], [4]. Their produced mechanical torque is built up from electromagnetic combinations of the permanent magnet and the reluctance created by the rotor's anisotropy. Because of their reluctance torque element, IPMSMs are considered well adequate for field-weakening operations; also, the IPMSMs' rotors have mechanical durability, which is essential for smaller air gaps and high-speed, high-torque operations [5]. The reluctance torque is a product of the saliency of a high quadrature inductance and of the direct inductance of the IPMSM. The saliency also gives interlinkage between the quadrature current and the direct current, a fact named ''cross-magnetization'' [6]. Besides a high magnetic saturation level, the IPMSM's behavior is particularly nonlinear because of the cross-magnetization effect [7], [8]. The stator inductances are dependent on armature current as a result of the magnetic saturation. Even more, the permanent magnet's flux variation is dependent on temperature changes. PMSM drives face several addresses that need to be addressed, such as the effects of the stator and rotor design ideas, expanded torque density, limited machine noise and vibration, high starting torque capability with comprehensive operating speed range, fault-tolerant, high speed and constant power operation area, and more [9]. Hence, the delicate control of the PMSM drive is a challenge that has augured researchers to develop sophisticated control technology to address it.

In [10], [11], and [12], model predictive control (MPC), which is based on the dynamic model of the plant, is used for direct speed control, avoiding the need for the complicated cascaded-control structure as it picks future speed conditions and selects a control action directly based on the speed tracking error. Similarly, in [2], MPC is used again for direct speed control along with a Lyapunov function to generate the space vector pulse width modulation (SVPWM) scheme's

The associate editor coordinating the review of this manuscript and approving it for publication was Jinquan Xu.

switching sequence. Another MPC technique, in [13], selects dynamically the voltage vectors by optimization, and various other MPC methods are also investigated in [14] and [15]. A model-free predictive current control (MFPCC) of an IPMSM is developed in [16] to eliminate the requirement for extensive prior knowledge of the system but it relies entirely on stator currents and current variations corresponding to different inverter switching states. Despite the MFPCC approach's significant differences, it uses a measure similar to that used in the model-based predictive current control (MBPCC) approach to derive the inverter's future switching state by minimizing a cost function.

But, MPC requires long-drawn manipulations through optimization to calculate the control action [17]. Another popular approach for IPMSM speed tracking is sliding mode control (SMC) owing to its ability to achieve robustness to numerous uncertainties such as parameter variations [18], [19]. The SMC and adaptive linear neuron (ADALINE) proportional resonant (PR) control is proposed as a straightforward reference current calculation that is not based on any complex filtering, mathematical transformation, or phase-locked loop in order to counteract the effects of unbalancing cases [20]. In spite of the good performance witnessed with these methods, their inherent chattering phenomenon emerging from large gains needed for robustness remains a significant drawback in many applications, limiting their broad use [21]. In [22], a disturbance observer (DO) is used to estimate the load torque. A state feedback controller with an integral term is developed at an operational point after a nonlinear PMSM model is linearized using the Jacobian linearization. In addition, this method is extended by using a sliding-mode observer with the DO in cascade for a speed sensorless operation. Adaptive control is considered a good alternative to cope with structured parameter variations due to varying operating conditions [23], [24], [25]. However, this technique is also known for not reckoning with the system's unmodeled dynamics and, hence, remains vulnerable to unstructured uncertainties like unpredictable load torque disturbance. Even so, it is practically not realistic to model mathematically every element of the evolving environment where IPMSM drives are deployed. Moreover, intelligent control does not have such a limitation due to its model-free characteristic. For instance, artificial neural networks are well-known for their learning capabilities. This feature was successfully used to learn systems with high nonlinearities and other types of uncertainties [26]. A thorough search for relevant literature reveals that intelligent control is used in PMSM drive applications that require robustness [24], [27], [28]. A major drawback, however, with this control philosophy is that it exhibits good performance at the expense of heavy computation [29]. This introduces some level of complication in the control design and makes their real-time implementation challenging.

In [30], a variable-equivalent-parameter MTPA control law is proposed. The effect of the machine parameters' variation is considered on the MTPA trajectory tracking. This strategy depends on current sensing to provide accurate MTPA current references. Also, MTPA control based on virtual signal injection (VSI) strategy can be applied to improve the efficiency of IPMSMs for EVs while inhibiting the noise of the IPMSM, that is compared against the traditional control strategy ($i_d = 0$) and look-up table (LUT) method [31], [32]. In [33], considering the difference between the voltage output by the current controller and the actual voltage applied to the motor helps to improve the accuracy of derivative information that influences the current references. Therefore, the tracking of the MTPA point based on VSI is more accurate than traditional methods. In [34], the scalar control (v/f) method is introduced as a modern MTPA method to control the PMSM. In this strategy, a sensorless method is proposed to control only the amplitude and frequency of the stator voltage vector without using any rotor positioner. In contrast, this methodology injects a high-frequency voltage signal into the stator current vector frame, which can be filtered from the measured currents. A nonlinear-PI (NPI) controller is utilized instead of the more common PI controller in order to improve the controller's convergence property [35]. Alternatively, a novel integrated control scheme, which combines the field-oriented control (FOC) scheme with the direct flux vector control (DFVC), is presented in [36]. This control method combines the advantages of both FOC and DFVC while avoiding the disadvantages of the two control methods. Hence, accurate MTPA control is achieved in the constant torque and power regions.

Unlike the aforementioned techniques, this manuscript proposes a simple MTPA speed control strategy for IPMSM drives. The direct voltage control scheme is able to make the IPMSM track a desired speed trajectory by varying the motor's voltage angle and amplitude with respect to torque and speed. This approach simplifies remarkably the control scheme with regard to conventional cascaded control methods like field-oriented control (FOC). Yet, the few direct voltage control attempts of PMSMs either require dc-link current sensing, inner stabilizing loop, or sophisticated control [29], [37], [38], [39], [40], [41], [42], [43], [44]. Studies have shown that finding optimum operation points with minimum current in the presence of various uncertainties requires extensive tuning [43]. In [44], genetic algorithm is utilized to determine the control gains at the expense of heavy computation. Furthermore, [45] uses a numerical approach to find the specific pair of (v, $\Delta\theta$) for IPMSM at different load torques and speeds.

To solve these limitations, the manuscript suggests a simple MTPA speed control strategy with a thorough insight analysis to determine analytically the control gains, which substantially simplifies the control and tuning to make it more suitable for low-cost real-time implementation as opposed to other methods. The proposed control method does not count on actual voltage values; therefore, acquiring the noisy motor's voltages is unnecessary. Also, unlike most existing

methods, the direct current control loops are not needed in the designed technique because it is based on the direct voltage control strategy, which indirectly regulates the machine current by limiting/controlling the desired voltage. In other words, the direct current control loop does not exist in the proposed method, no direct current controller. Comparisons are conducted experimentally against the popular MTPA field-oriented vector control to illustrate the simplicity and effectiveness of the proposed MTPA controller. To the best of the authors' knowledge, this is the first attempt at achieving MTPA for IPMSMs using a single PI controller with insight analysis to determine the control gains.

The remaining portion of the manuscript is laid out as follows: Section II presents the vehicle model and Section III describes the IPMSM's dynamics. The suggested controller is outlined in Section IV. Finally, Section V reports and analyzes experimental comparative results.

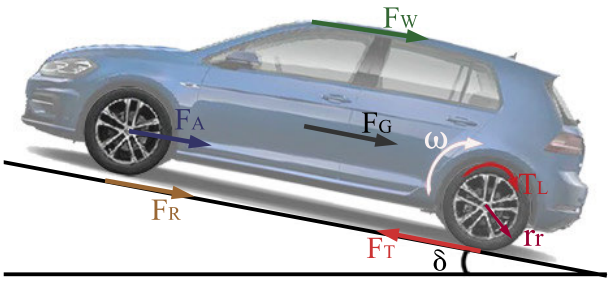

FIGURE 1. Vehicle dynamic model for resistance forces calculation.

II. VEHICLE MODEL

Typical resistance forces for a moving vehicle include wind resistance F_W resulting from air and vehicle interaction, rolling resistance F_R resulting from tire and road interaction, grade resistance F_G resulting from different road grades, and acceleration resistance F_A resulting from the need to accelerate the mass of the vehicle. The total tractive force for the vehicle is shown in Fig. 1 and specified in (1), [46],

$$F_T = F_R + F_W + F_G + F_A \tag{1a}$$

$$F_T = K_R W\cos(\delta) + K_W A V^2 + W\sin(\delta) + W\frac{a}{g} \tag{1b}$$

where,

K_R	Rolling resistance coefficient
K_W	Wind resistance coefficient
δ	Road grade angle
W	Vehicle weight
V	Vehicle speed
A	Vehicle frontal area
a	Vehicle acceleration
g	Gravitational constant

It might be challenging to accurately describe how torque and vehicle speed change under all possible traffic scenarios. Various standard driving cycles have been enhanced to simulate actual traffic conditions. The EPA Supplemental Federal Test Procedure (*US*06) is one of them. The following equations are used to calculate the motor's reference input values (speed ω, torque τ_L) after the tractive force F_T has been determined from (1),

$$\omega^* = \frac{r_f}{r_r}V \tag{2a}$$

$$\tau_L = \frac{r_r}{r_f}F_T \tag{2b}$$

where, r_f is gear ratio and r_r is rolling radius of the wheel.

The standard driving cycle serves as the input, and the speed tracking and armature current serve as the output for the EV powertrain model. Between this model's input and output, there are: Initially, a vehicle model is used, which converts the driving cycle into speed and torque values for the reference motor. Then, the motor control model is built to track the MTPA trajectory according to the reference speed and torque [45].

III. IPMSM DYNAMICS

The dynamic model of an IPMSM in the rotating reference frame $d-q$ can be written as [29]:

$$v_d = Ri_d + L_d\frac{d}{dt}i_d - L_q p\omega i_q \tag{3a}$$

$$v_q = Ri_q + L_q\frac{d}{dt}i_q + L_d p\omega i_d + p\lambda\omega \tag{3b}$$

$$\tau = \frac{3}{2}p\Big[(L_d - L_q)i_d i_q + \lambda i_q\Big] \tag{3c}$$

The mechanical equations describing the IPMSM's motion can be written as:

$$\frac{d}{dt}\omega = \frac{1}{J}(\tau - F_v\omega - \tau_L) \tag{4a}$$

$$\frac{d}{dt}\theta = p\omega \tag{4b}$$

where, v_d, v_q, and i_d, i_q are the direct and quadrature stator voltage and current, L_d, L_q is the inductance in $d-q$ coordinates, R is the armature winding resistance, λ is the stator flux linkage due to the permanent magnets (PM), J is the rotor and load inertia, p is the number of pole pairs, F_v is the viscous friction coefficient, θ and ω are the electrical position and mechanical speed, respectively, τ and τ_L represent the motor and load torques, respectively. From (4), the mechanical equations of motion, the motor torque equals the frictional and load torques at steady-state. The load torque, which is affected by the mechanical load or the road/driving conditions, has a direct influence on the motor torque/current.

IV. MTPA SPEED CONTROL APPROACH

From [42], the IPMSM's dynamics (3) at steady-state can be expressed in a linear matrix form:

$$\begin{bmatrix} v_d \\ v_q \end{bmatrix} = \begin{bmatrix} R & -p\omega L_q \\ p\omega L_d & R \end{bmatrix}\begin{bmatrix} i_d \\ i_q \end{bmatrix} + \begin{bmatrix} 0 \\ p\omega\lambda \end{bmatrix} \tag{5}$$

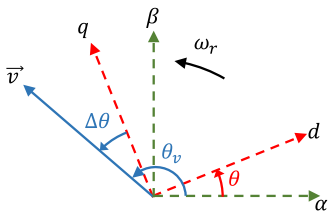

FIGURE 2. Spatial relationship between the applied voltage vector and reference frames.

Using (5), the motor's currents can be described in term of voltages [42]:

$$\begin{bmatrix} i_d \\ i_q \end{bmatrix} = k_1 \begin{bmatrix} R & p\omega L_q \\ -p\omega L_d & R \end{bmatrix} \begin{bmatrix} v_d \\ v_q - p\omega\lambda \end{bmatrix}$$
$$\text{where,} \quad k_1 = \frac{1}{R^2 + p^2\omega^2 L_d L_q} \tag{6}$$

k_1 is the determinant of the parameter matrix. Thus, the motor's q-axis current can be expressed by,

$$i_q = k_1\Big(Rv_q - p\omega L_d v_d - Rp\omega\lambda\Big) \tag{7}$$

Setting $v_d = -v\sin(\Delta\theta)$ and $v_q = v\cos(\Delta\theta)$ leads to,

$$i_q = k_1\Big(Rv\cos(\Delta\theta) + p\omega L_d v\sin(\Delta\theta) - Rp\omega\lambda\Big) \tag{8}$$

Where, v and θ_v are the voltage amplitude and angle, respectively. The spatial correlation between the synchronously rotating $d-q$ frame, $\alpha-\beta$ stationary frame, and applied voltage vector is depicted in Fig. 2. Where $\theta_v = \theta + \Delta\theta + \pi/2$, and $\Delta\theta$ is the contribution of the proposed method's controller.

MTPA is used to produce the output torque with minimal current consumption. Since the minimization of the stator current amplitude is required, the torque derivative with respect to the angle of the current is calculated [5],

$$i_d = \frac{-\lambda + \sqrt{\lambda^2 + 4(L_d - L_q)^2 i_q^2}}{2(L_d - L_q)} \tag{9}$$

Substituting i_q from (8) in (9) yields to (10), as shown at the bottom of the page. Then, by substituting i_q and i_d, respectively, from (8) and (10) in (3c), the motor's torque at MTPA can be expressed directly in terms of its voltage amplitude v and angle $\Delta\theta$ as described by (11), as shown at the bottom of the page.

It is important to note that the target torque (11) at MTPA operation condition is expressed in terms of its voltage amplitude v, angle $\Delta\theta$ and speed ω. The MTPA control objective is to generate an optimal pair of v and $\Delta\theta$ for a specified torque/speed condition. It is noteworthy that there are infinite possibilities of the pairs (v, $\Delta\theta$) to satisfy a given torque/speed condition. However, these pairs come with different current amplitudes and various losses. Therefore, the MTPA control aim is to find the specific pair (v, $\Delta\theta$) with the minimum current consumption. It is also important to note that expressing mathematically the optimal pairs (v, $\Delta\theta$) as a function of torque τ and speed ω from (11) is a difficult task to undertake. Consequently, Fig. 3 illustrates the optimal pairs of (v, $\Delta\theta$) from (11) at different load torque and speed.

Fig. 3(b) describes the correlation between the applied voltage's magnitude and the motor's speed. As it can be seen, the applied voltage's magnitude, for a specific load torque, changes linearly with the motor's speed. As the load torque increases, the needed voltage amplitude also increases to cope with a higher load and maintain the motor's speed. Henceforth, the voltage-speed relationship could be designated as a straight proportionality with respect to the load torque. The curve slope converts its rate at no-load to its maximum rate at the nominal load torque of the motor.

Fig. 3(d) presents the relationship between the voltage's angle and the load torque. As seen, there is a nonlinear correlation such that the voltage angle, for a given motor's speed, can be modeled as a function of the square root of the applied torque. As speed rises, a change in curvature is observed, indicating an increase in the constant of proportionality at low speeds only. Furthermore, the PI controller compensates for any parameter change that directly affects $\Delta\theta$ calculation. Along with the direct effect of parameter changes on machine current, which reflects on torque calculation (3c), the voltage magnitude value varies to handle the mechanical load while keeping the motor's speed.

From [47], to obtain the maximum torque at minimum stator current, i_d can be written simply in terms of i_q for MTPA operating point for IPMSM drives as:

$$i_d = \frac{(L_d - L_q)}{\lambda} i_q^2 \tag{12}$$

Substituting i_d in (3c) yields:

$$\tau = \frac{3}{2}p\Big[\frac{(L_d - L_q)^2}{\lambda} i_q^3 + \lambda i_q\Big] \tag{13}$$

where τ is written in terms of i_q only. equation (13) can be rewritten as:

$$\frac{3}{2}p\Big[\frac{(L_d - L_q)^2}{\lambda} i_q^3 + \lambda i_q\Big] - \tau = 0 \tag{14}$$

Which is a depressed cubic equation in terms of i_q. This equation has 2 imaginary roots and 1 real root. Hence, the

$$i_d = \frac{-\lambda + \sqrt{\lambda^2 + 4(L_d - L_q)^2 (k_1(Rv\cos(\Delta\theta) + \omega L_d v\sin(\Delta\theta) - R\omega\lambda))^2}}{2(L_d - L_q)} \tag{10}$$

$$\tau = \frac{3}{4}pk_1\Big(Rv\cos(\Delta\theta) + \omega L_d v\sin(\Delta\theta) - R\omega\lambda\Big)\Big(\lambda + \sqrt{\lambda^2 + 4(L_d - L_q)^2 (k_1(\omega L_d v\sin(\Delta\theta) + Rv\cos(\Delta\theta) - R\omega\lambda))^2}\Big) \tag{11}$$

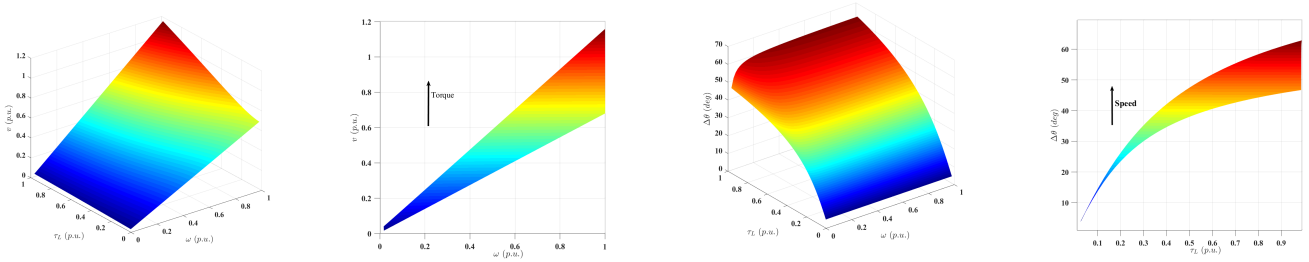

FIGURE 3. Performance features of the IPMSM: (a) and (b) Voltage amplitude vs. torque load and speed; (c) and (d) Voltage angle vs. torque load and speed.

real root can be found using Cardano's Method, which gives,

$$i_q = \sqrt[3]{A\tau + B\sqrt{C\tau^2 + D}} - \sqrt[3]{-A\tau + B\sqrt{C\tau^2 + D}} \quad (15)$$

where:

$$A = \frac{\lambda}{3p(L_d - L_q)^2} \quad (16a)$$

$$B = \frac{\lambda}{3(L_d - L_q)^2} \quad (16b)$$

$$C = \frac{1}{p^2} \quad (16c)$$

$$D = \frac{\lambda^4}{3(L_d - L_q)^2} \quad (16d)$$

Remarkably, A, B, C and D are dependent on motor's parameters, assuming a constant motor model, which makes i_q dependent on τ only. Thus, from (5), the motor's voltage magnitude can be explained as follows,

$$v = \sqrt{v_d^2 + v_q^2} \quad (17)$$

$$v = \sqrt{(Ri_d - L_q p\omega i_q)^2 + (Ri_q + L_d p\omega i_d + p\lambda\omega)^2} \quad (18)$$

and the voltage angle deflection from the quadrature axis is given by:

$$\Delta\theta = -\tan^{-1}\left(\frac{v_d}{v_q}\right) = -\tan^{-1}\left(\frac{Ri_d - L_q p\omega i_q}{Ri_q + L_d p\omega i_d + p\lambda\omega}\right) \quad (19)$$

Substituting (12) and (15) in (18) and (19) yield the motor's voltage amplitude v and the angle $\Delta\theta$ at MTPA as a function of speed and torque, i.e., equation (20) and (21), as shown at the bottom of the page.

MTPA is applied to enhance the output torque in the stable torque region of the motor. Notwithstanding, using (20) and (21) are sophisticated and hard to programing them and

$$v = \sqrt{\left[R\frac{(L_d - L_q)}{\lambda}\left(\sqrt[3]{A\tau + B\sqrt{C\tau^2 + D}} - \sqrt[3]{-A\tau + B\sqrt{C\tau^2 + D}}\right)^2 - L_q p\omega\left(\sqrt[3]{A\tau + B\sqrt{C\tau^2 + D}} - \sqrt[3]{-A\tau + B\sqrt{C\tau^2 + D}}\right)\right]^2} + \left[R\left(\sqrt[3]{A\tau + B\sqrt{C\tau^2 + D}} - \sqrt[3]{-A\tau + B\sqrt{C\tau^2 + D}}\right) + L_d p\omega\frac{(L_d - L_q)}{\lambda}\left(\sqrt[3]{A\tau + B\sqrt{C\tau^2 + D}} - \sqrt[3]{-A\tau + B\sqrt{C\tau^2 + D}}\right)^2 + p\lambda\omega\right]^2 \quad (20)$$

$$\Delta\theta = -\tan^{-1}\left(\frac{R\frac{(L_d - L_q)}{\lambda}\left(\sqrt[3]{A\tau + B\sqrt{C\tau^2 + D}} - \sqrt[3]{-A\tau + B\sqrt{C\tau^2 + D}}\right)^2 - L_q p\omega\left(\sqrt[3]{A\tau + B\sqrt{C\tau^2 + D}} - \sqrt[3]{-A\tau + B\sqrt{C\tau^2 + D}}\right)}{R\left(\sqrt[3]{A\tau + B\sqrt{C\tau^2 + D}} - \sqrt[3]{-A\tau + B\sqrt{C\tau^2 + D}}\right) + L_d p\omega\frac{(L_d - L_q)}{\lambda}\left(\sqrt[3]{A\tau + B\sqrt{C\tau^2 + D}} - \sqrt[3]{-A\tau + B\sqrt{C\tau^2 + D}}\right)^2 + p\lambda\omega}\right) \quad (21)$$

$$i_q = \sqrt[3]{2\frac{\lambda}{3p(L_d - L_q)^2}\tau} \quad (22)$$

$$v = \sqrt{\frac{4R}{3}\omega\tau + p^2\lambda^2\omega^2 + Z_d^2\sqrt[3]{\left(\frac{4\tau^2}{9p^2\lambda(L_d - L_q)}\right)^2} + \omega^2\sqrt[3]{\left(\frac{2p^2\lambda(L_d - L_q)\tau}{3}\right)^2}} \quad (23)$$

$$\Delta\theta = -\tan^{-1}\left(\frac{R\frac{(L_d - L_q)}{\lambda}\sqrt[3]{\left(\frac{2\lambda\tau}{3p(L_d - L_q)^2}\right)^2} - L_q p\omega\sqrt[3]{\frac{2\lambda\tau}{3p(L_d - L_q)^2}}}{R\sqrt[3]{\frac{2\lambda\tau}{3p(L_d - L_q)^2}} + L_d p\omega\frac{(L_d - L_q)}{\lambda}\sqrt[3]{\left(\frac{2\lambda\tau}{3p(L_d - L_q)^2}\right)^2} + p\lambda\omega}\right) \quad (24)$$

$$v = \sqrt{(L_q p\omega)^2 i_q^2 + \frac{(L_d p\omega)^2(L_d - L_q)^2}{\lambda^2} i_q^4 + (p\lambda\omega)^2 + 2L_d(p\omega)^2(L_d - L_q)i_q^2} \quad (25)$$

do not worthwhile for industrial applications. Since the idea is to reduce the stator current magnitude, in equation (15), the high order of $\sqrt[6]{\frac{\lambda^4}{3(L_d-L_q)^2}} \approx 0$; so that D becomes negligible, which leads to the motor's q-axis current expressed by (22), as shown at the bottom of the previous page.

On the other hand, setting $Z_d^2 = R^2 + (L_d p\omega)^2$ and by substituting i_q from (22) in (20) and (21), the applied voltage amplitude v and angle $\Delta\theta_v$ at MTPA can be expressed directly in terms of motor's speed ω and torque τ as described by (23) and (24), as shown at the bottom of the previous page.

It is noteworthy that expressing the motor's voltage magnitude and angle at MTPA in terms of its speed and torque is still complicated. Furthermore, studies have shown that the mechanical time constant is much more dominant than its electric counterpart. Thus, the voltage drop due to the motor's resistance has a negligible impact, [44]; therefore, applying that on (18) with considering of (12) leads to (25), as shown at the bottom of the previous page.

While $\frac{(L_d-L_q)}{\lambda} \ll 1$; therefore, the high order of this term is negligible. $\Rightarrow \frac{(L_d-L_q)^2}{\lambda^2} \approx 0$, so,

$$v = p\omega\lambda\sqrt{1+\left(\frac{L_d^2+(L_d-L_q)^2}{\lambda^2}\right)i_q^2} \tag{26}$$

Equation (26) can be simplified by using Taylor Series expansion around zero as,

$$v = \omega\left(p\lambda + \frac{p}{\lambda}\frac{L_d^2+(L_d-L_q)^2}{2}i_q^2\right) \tag{27}$$

The equation (22) can be rewritten as,

$$i_q^2 = \left(\frac{2\lambda}{3p(L_d-L_q)^2}\right)^{2/3}\tau^{2/3} \tag{28}$$

Using (28) in the current form leads to some computing delay in finding the voltage amplitude value, which has an impact on the speed tracking performance. Therefore, equation (28) can be simplified to avoid any latency lag by employing the Maclaurin Series as,

$$i_q^2 = \frac{1}{3}\left(\frac{2\lambda}{3p(L_d-L_q)^2}\right)^{2/3}(1+2\tau) \tag{29}$$

By substituting i_q^2 (29) in v equation (27) yields,

$$v = \omega\left(p\lambda + \frac{p}{\lambda}\frac{L_d^2+(L_d-L_q)^2}{6}\left(\frac{2\lambda}{3p(L_d-L_q)^2}\right)^{2/3}(1+2\tau)\right) \tag{30}$$

As it can be read from (30), the applied voltage's magnitude, for a specific load torque, changes linearly with the motor's speed. As the load torque increases, the needed voltage amplitude also increases to cope with a higher load and maintain the motor's speed. Thus, the motor's voltage amplitude is defined as,

$$v = \left(K_{v1} + K_{v2}(1+2\tau)\right)\omega^* \tag{31}$$

where:

$$K_{v1} = p\,\lambda \tag{32a}$$

$$K_{v2} = \frac{p}{\lambda}\frac{L_d^2+(L_d-L_q)^2}{6}\left(\frac{2\lambda}{3p(L_d-L_q)^2}\right)^{2/3} \tag{32b}$$

From (19), $\Delta\theta$ is small angle deviation such as $\tan^{-1}(x) \approx x$, [48]; accordingly, the angle deflection from the q-axis $\Delta\theta$ is rewritten as,

$$\Delta\theta = \frac{L_q p\omega i_q}{L_d p\omega\frac{(L_d-L_q)}{\lambda}i_q^2 + p\lambda\omega} \tag{33}$$

While $\frac{(L_d-L_q)}{\lambda} \ll 1 \Rightarrow \approx 0$; then,

$$\Delta\theta = \frac{L_q}{\lambda}i_q \tag{34}$$

Substituting i_q (29) in $\Delta\theta$ equation (34) yields,

$$\Delta\theta = \frac{L_q}{\lambda}\frac{1}{\sqrt{3}}\sqrt[3]{\frac{2\lambda}{3p(L_d-L_q)^2}}\sqrt{1+2\tau} \tag{35}$$

As it can be seen in (35), there is a nonlinear correlation that the voltage's angle, for a given motor's speed. Therefore, the motor's voltage angle variation is defined as,

$$\Delta\theta = K_\theta\sqrt{1+2\tau} + \Delta\theta_{FBK} \tag{36}$$

where, $\Delta\theta_{FBK} = K_p\,e_\omega + K_i\int e_\omega$

$$K_\theta = \frac{L_q}{\lambda}\frac{1}{\sqrt{3}}\sqrt[3]{\frac{2\lambda}{3p(L_d-L_q)^2}} \tag{37}$$

Since a feedforward would eventually result in residual errors due to various uncertainties, a simple proportional-integral (PI) controller is added as feedback. Given a predefined reference speed trajectory ω^*, an error of speed tracking is outlined by $e_\omega = \omega - \omega^*$. The error signal is applied to the PI controller that drives the error to zero by effecting proper action. The PI control gains K_p and K_i are chosen using empirical analysis; however, the analytical method is used as an insight for the selection of the values for the coefficients K_{v1}, K_{v2} and K_θ.

The control scheme is illustrated in Fig. 4. At is can be seen, the controller drives the motor's speed to its desired trajectory by providing the desired voltage's amplitude v and angle $\Delta\theta$ which are then applied to a space vector pulse width modulation (SVPWM) module to produce the essential gate pulses required by the inverter.

Henceforth, the simplified motor's voltage amplitude and angle variation are defined in (31) and (36), with the control coefficients K_{v1}, K_{v2} and K_θ calculated as in (32) and (37). Unlike other methods where control gains are set using an extensive trial-and-error procedure, formulation (32) and (37) provide an analytical solution to calculate these gains. This is important to note that gains are expressed in terms of the motor's parameters, which provides an insight for further tuning. The proposed strategy exploits the simple relationship

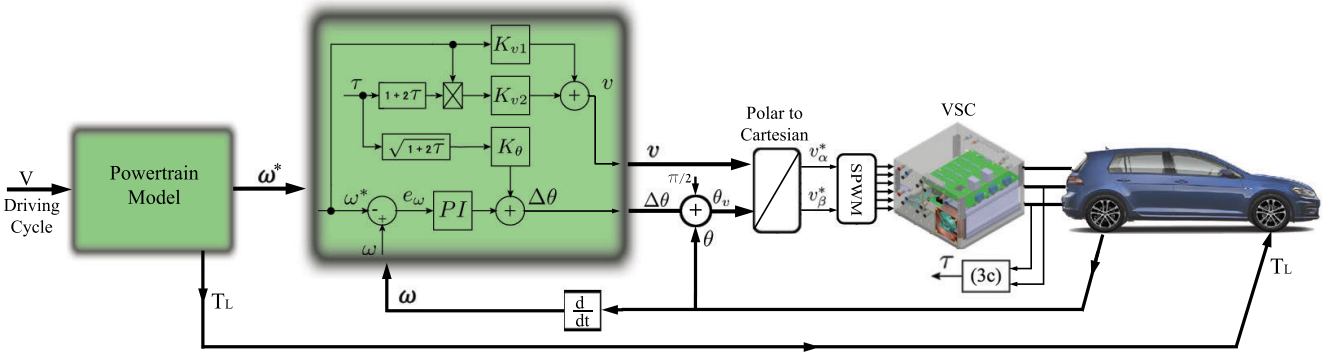

FIGURE 4. Control scheme.

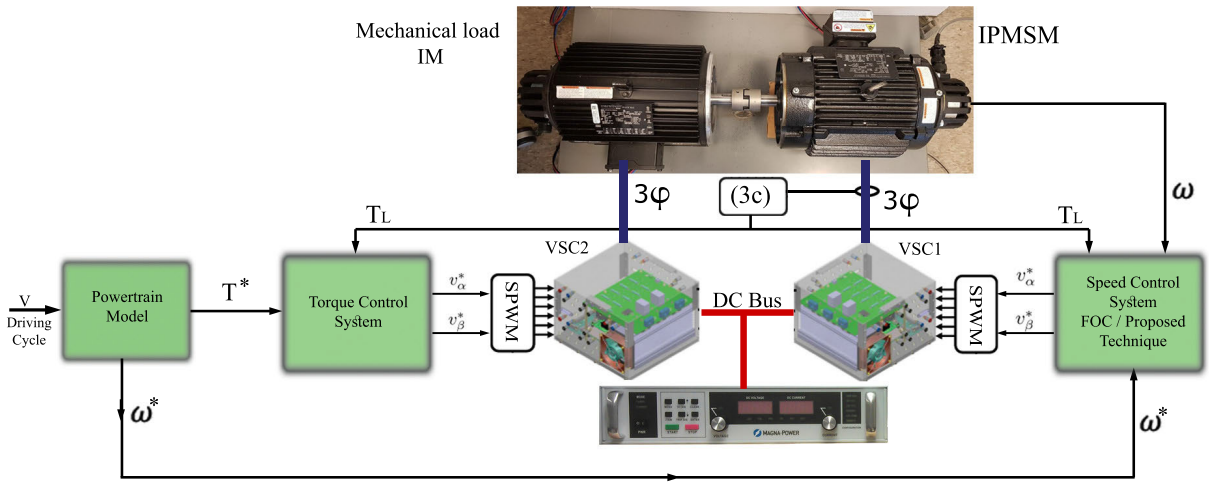

FIGURE 5. Experimental electric vehicle 5Hp motors setup.

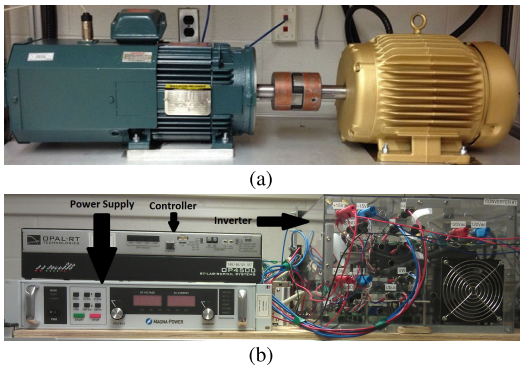

FIGURE 6. Experimental setup.

between voltage, speed and torque depicted in Fig. 3. Since the load torque can be directly estimated from (3c), no current control regulation is needed.

V. VALIDATION AND DISCUSSION

A. EXPERIMENTAL IPMSM SETUP

To assess the performance of the MTPA controller, various tests are conducted on 7.46 KW/10 HP and 3.7 KW/5 HP,

TABLE 1. 10HP Motor's physical parameters.

Parameter	value
Nominal power (KW/Hp)	$P_n = 7.46/10$
Nominal speed (RPM)	$w_n = 1800$
Nominal torque (N·m)	$\tau_n = 39.5$
Direct inductance (H)	$L_d = 22.1 \cdot 10^{-3}$
Quadrature inductance (H)	$L_q = 91.1 \cdot 10^{-3}$
Armature winding resistance (Ω)	$R = 6.51 \cdot 10^{-1}$
Flux linkage (Wb)	$\lambda = 67.09 \cdot 10^{-2}$
Number of pole pairs	$p = 2$

1800 RPM IPMSMs, (Table 1 and 2). The motors parameters have been used from the manufacturer's data sheet after adjusting the parameters according to lab temperature and confirming the result with the measured values. As depicted in Fig. 5 and 6, induction motors of the same power are controlled in torque mode to generate the mechanical load while the IPMSM operates in speed mode through the inverter. A DC power supply is used to produce a stabilized voltage of 750/350 Vdc. The sampling and switching frequencies are set to 20 kHz and 1 kHz, respectively. The experiment setup is modeled in the MATLAB/Simulink environment and implemented in a real-time OP4500 platform and a Texas

TABLE 2. Vehicle parameters.

Parameter	Value
Vehicle mass (p.u)	$M_v = 1.0$
Vehicle frontal area (m^2)	$A = 2.35$
Rolling resistance coefficient: for average paved roads	$K_R = 0.015$
Wind resistance coefficient ($N/(m^2/s)^2$): for passenger cars	$K_W = 0.3$
Gear ratio	$r_f = 1.0$
Wheel rolling radius (m)	$r_r = 0.325$
Nominal motor power (KW/Hp/p.u)	$P_n = 3.7/5/1.0$
Nominal motor speed (RPM/p.u)	$w_n = 1800/1.0$
Nominal motor torque (N·m/p.u)	$\tau_n = 19.8/1.0$
Nominal motor line voltage (V)	$v_n = 230$
Inductance in d-axis (H)	$L_d = 4.2 \cdot 10^{-3}$
Inductance in q-axis (H)	$L_q = 8.3 \cdot 10^{-3}$
Armature winding resistance (Ω)	$R = 0.2$
Flux linkage (Wb)	$\lambda = 10.8 \cdot 10^{-2}$
Number of pole pairs	$p = 3$

Instruments DSP card (F28379D). The control performance is evaluated taken into account the motor's three-phase currents, speed tracking signals, voltage amplitude and angle variation, the control signal, and duty cycles, i.e., applied voltage $v^*_{\alpha\beta}$. The speed and torque compensation gains are chosen using (32), (37).

B. DRIVING CYCLE VALIDATION

The vehicle model presented in Section II is executed for EPA Supplemental Federal Test Procedure (*US*06) driving cycle. The standard driving cycle utilized for experimental validation is a driving pattern for automotive dynamometers that captures vehicle dynamics. The driving profiles, motor reference speed, and mechanical load torque of the scaled machine without regenerative braking are created using the vehicle and IPMSM data in Table 2 [49]. Fig. 5 shows the experimental setup of the electric vehicle model, which contains the driving IPMSM motor and induction dyno motor, along with the powertrain model. The powertrain model's output speed is the reference speed of the FOC or proposed speed control system, and the torque output is the reference torque of the dyno motor control system. Each control system operates an independent voltage source inverter to drive its respective motor.

The driving cycle experimental comparison is presented to confirm the advantages of the simple direct voltage control model over the FOC method and avoid its limitation for electric vehicle use. Therefore, the proposed method is proved by matching it with the FOC MTPA method at the same speed/torque reference trajectory, at *US*06 standard driving cycle with a real-time simulation pattern. The machine performance is presented in Fig. 7 for both proposed and FOC MTPA strategies. The speed reference trajectory tracking for both methods and torque command are shown

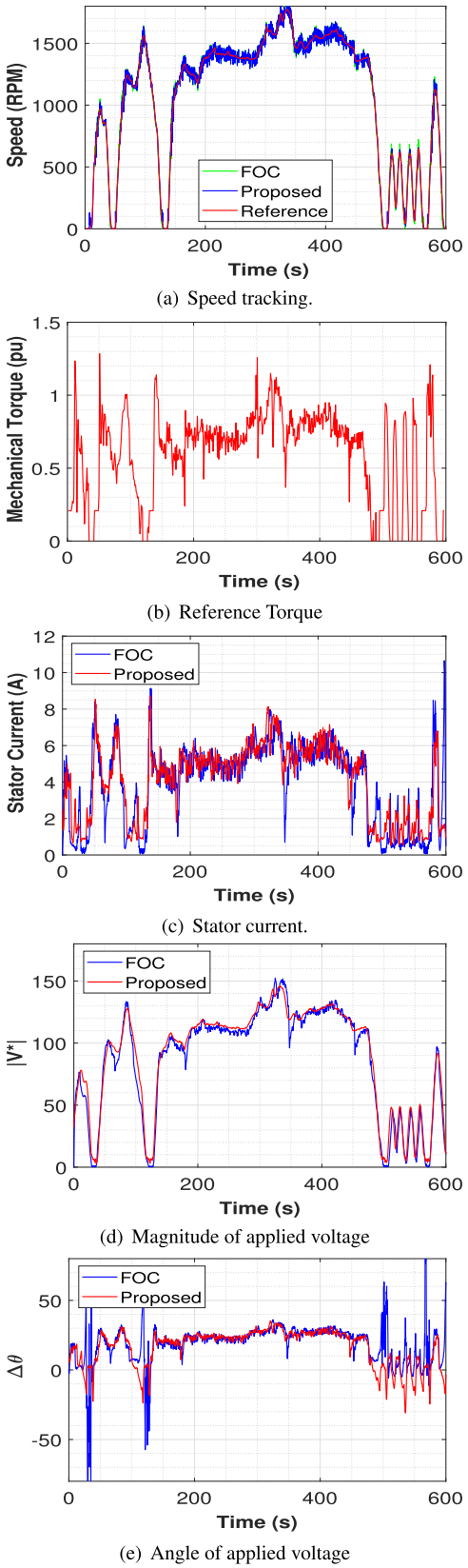

(a) Speed tracking.

(b) Reference Torque

(c) Stator current.

(d) Magnitude of applied voltage

(e) Angle of applied voltage

FIGURE 7. Experimental results with EPA Supplemental Federal Test Procedure (US06) Driving Cycle for 5HP IPMSM.

in Fig. 7(a) and 7(b). As it can be noticed, both strategies show perfect speed tracking implementation in the steady-state and transient situations during the driving cycle period. The proposed control strategy is qualified to provide a good response to the unpredicted changes in the load torque. Since this strategy directly controls the machine voltage, it avoids the delay of the cascade control chain effect of the FOC method. Also, the stator RMS current waveform confirms the good current consumption with a higher current impulse in the FOC than the proposed method during the transient state, Fig. 7(c). Moreover, the impact of the proposed design seems evident on the controller output signals, voltage's amplitude v Fig. 7(d) and voltage's angle $\Delta\theta$ Fig.7(e).

The simplicity of the suggested control approach must be investigated further since these assumptions may impact other IPMSM operating features. Fig. 7(d) compares the voltage amplitude of the IPMSM, which is a function of speed and load torque for the simplified technique (31) versus the FOC method, a non-simplified version with no assumptions. According to Fig. 7(d), both curves overlap in the machine's operating zone; however, they vary at some speed/load values due to disregarding higher order terms. Furthermore, Fig. 7(e) depicts the IPMSM voltage angle for the FOC method and the simplified proposed technique (36) (voltage angle as a function of speed and load torque). A nonlinear relationship exists between the voltage angle and the speed and torque of the motor. To compensate for the factors in (21) that are disregarded in order to keep the motor on the MTPA trajectory and the nonlinearity, a recovery voltage angle, $\Delta\theta_{FBK}$, is considered. As a result, the speed tracking curve, Fig. 7(a), confirms the acceptable performance of the proposed direct voltage control method.

C. GENERAL VALIDATION

The 2^{nd} machine (7.46 KW/10 HP, 1800 RPM IPMSM, Table 1) is tested at different operating conditions to assess the proposed control method's performance robustness and prove its generalization. A benchmark control method, FOC, is used to rate the effectiveness of the MTPA controller; the IPMSM drive is first controlled using the well-established MTPA vector control technique. A 24 N·m load torque is applied at 25 s and removed at 45 s, and performance is reported in Fig. 8. From Fig. 8(a), accurate speed tracking can be deduced by this control method. However, the controller is unable to obtain a level regulation of the applied voltage's angle, as it can be seen in Fig. 8(c). This can be attributed to the fact that the angle is not a directly controlled state, hence the irregular dynamics.

With the same reference speed trajectory as in the previous experiment, the suggested MTPA speed controller is subjected to a load torque disturbance of 24 N·m and the results are depicted in Fig. 9. As it can be seen, the proposed approach reveals good tracking behavior along with excellent current consumption (Fig. 9(b) and 9(d)). First, from Fig. 9(a), the speed increases when applying load torque and releasing it in the proposed method. This differs from the FOC method, Fig. 8(a), because the presented approach uses only one PI controller and avoids the delay of using the cascaded PI controller. The effect of the single PI is clearly seen in the parameters of the direct voltage control method (v, $\Delta\theta$), Fig. 9(c). The voltage angle and amplitude are immediately increased/decreased at applying/releasing the mechanical load, compared to Fig. 8(c). Second, from Fig. 9(d), the d-q axis currents prove the performance effectiveness of the direct voltage control strategy in tracking the MTPA trajectory by matching it with the proven FOC MTPA method, Fig. 8(d). It is remarkable that the controller can handle the load torque without any disproportionate current consumption. Therefore, MTPA operation can be achieved with direct voltage control.

TABLE 3. Sensitivity analysis for 10HP IPMSM.

Sensitivity	+30%	-50%
$S_\omega^{L_d}$	$3.7 \cdot 10^{-3}$	$2.78 \cdot 10^{-3}$
$S_\omega^{L_q}$	$1.85 \cdot 10^{-3}$	$11.1 \cdot 10^{-3}$
S_ω^{λ}	$1.31 \cdot 10^{-2}$	$1.56 \cdot 10^{-2}$
	+30%	-20%
$S_\omega^{R_s}$	$3.7 \cdot 10^{-4}$	$2.71 \cdot 10^{-4}$

To inspect the performance under an arbitrary speed/torque profile, an additional experiment is conducted. For that, the speed is changed from 0 to 50%, 100%, 75%, and 25% of the rated speed before being brought back to zero. The load torque is put in at 50% of the rated speed and, subsequently changed twice at the rated speed. Results are reported in Fig. 10 and 11. As it is depicted in Fig. 10(a) and 11(a), both methods show great speed control performance. In Fig. 10(d) and 11(d), satisfactory MTPA trajectory tracking is achieved in different operating conditions. In second place, the direct voltage control method presents good achievement in the mid-speed loaded case study (between 5-20s).

To assess the proposed control method's performance robustness to the machine's parameters variation, the parameters L_d, L_q are changed by $(+30\% - 50\%)$, R by $(+30\% - 20\%)$, and λ by $(+30\% - 50\%)$ between $25 - 40s$, $45 - 60s$, $65 - 80s$, and $85 - 100s$, respectively with nominal load torque. As it is shown in Fig. 12, adequate MTPA trajectory tracking is achieved in these operating conditions. As it can be observed in Fig. 12(a), the control performance seems to be more sensitive to a change in the flux that occurs from $85s$ to $100s$. This is expected since the control coefficients in (32) are linked to the flux. Nevertheless, the -50% flux variation generates less than 14 RPM deviation from rated speed which is an acceptable 0.8% error.

To further analyze the performance of the proposed methods, a sensitivity analysis is presented as the function given by [50],

$$S_f^p = \frac{df}{dp}\frac{p}{f} \tag{38}$$

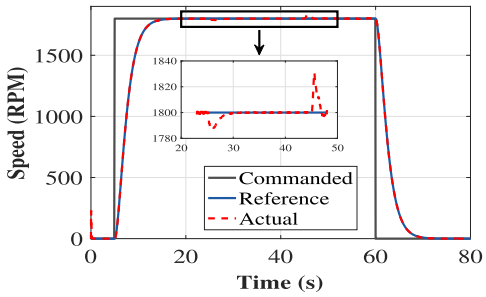

(a) Speed tracking.

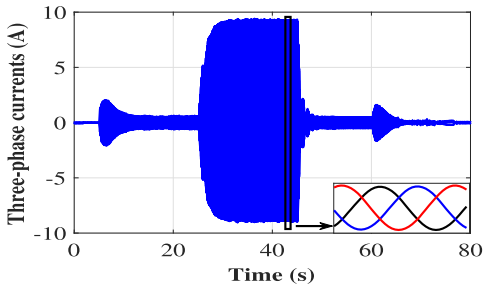

(b) Three-phase currents.

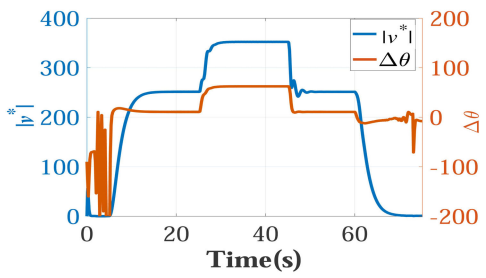

(c) Magnitude and angle

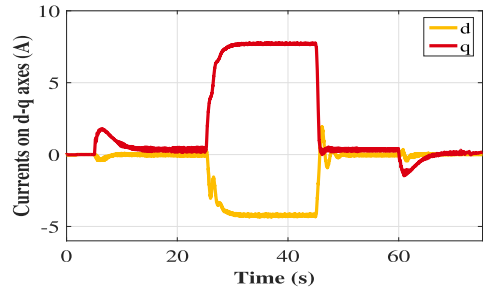

(d) i_{dq} currents

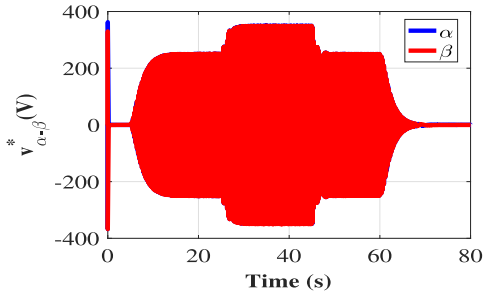

(e) Voltages in the α-β frame

FIGURE 8. Experimental results: MTPA FOC under 24 N·m for 10HP IPMSM.

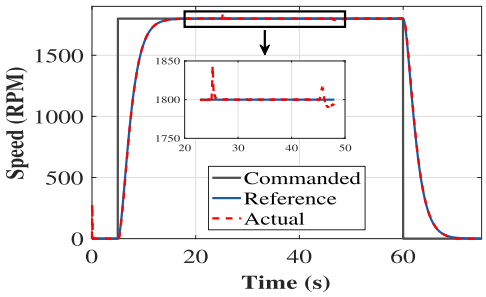

(a) Speed tracking.

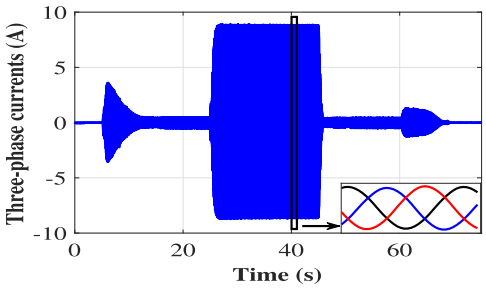

(b) Three-phase currents.

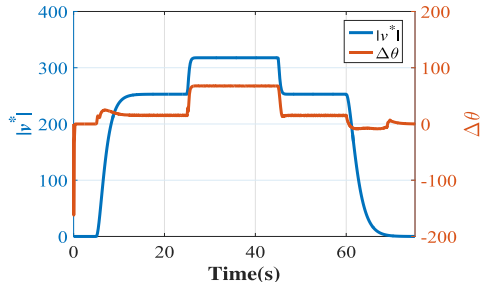

(c) Magnitude and angle

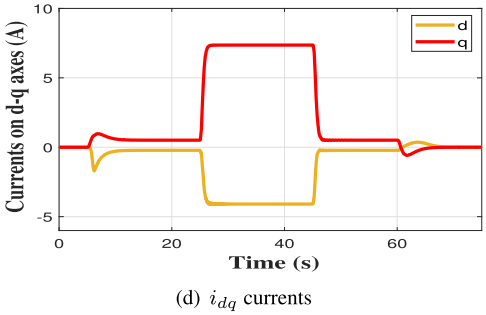

(d) i_{dq} currents

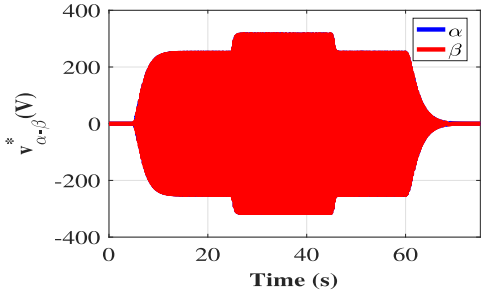

(e) Voltages in the α-β frame

FIGURE 9. Experimental results: proposed MTPA method under 24 N·m for 10HP IPMSM.

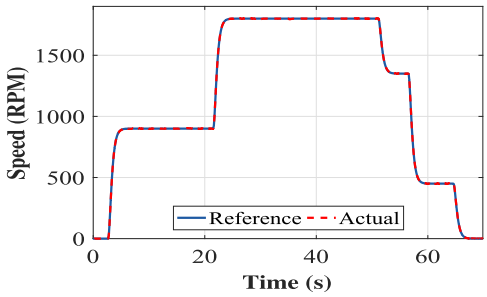

(a) Speed tracking.

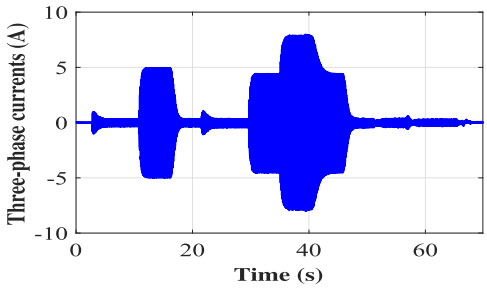

(b) Three-phase currents.

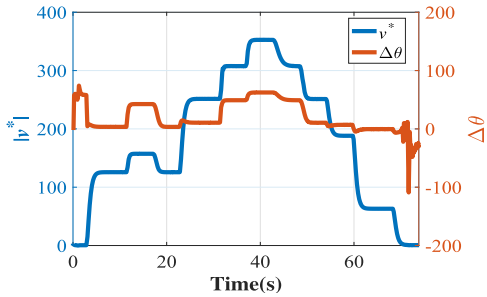

(c) Magnitude and angle

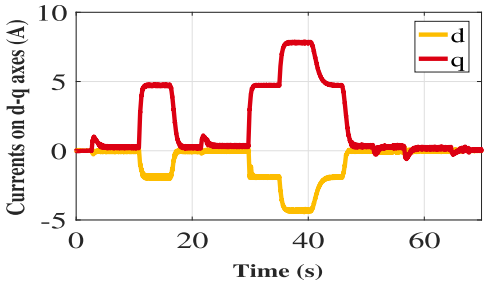

(d) i_{dq} currents

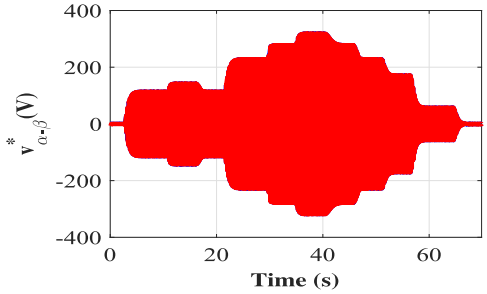

(e) Voltages in the α-β frame

FIGURE 10. Experimental results: MTPA FOC at random speed/torque for 10HP IPMSM.

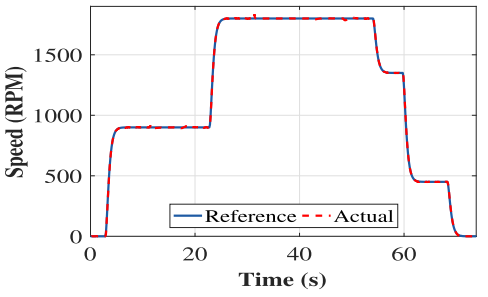

(a) Speed tracking.

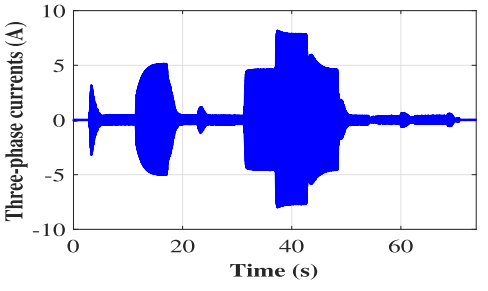

(b) Three-phase currents.

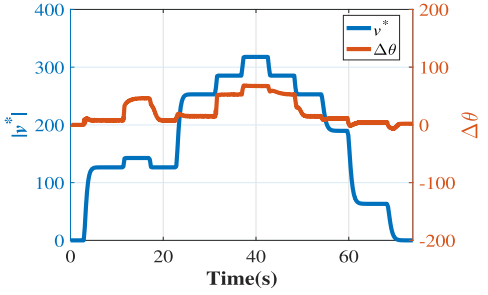

(c) Magnitude and angle

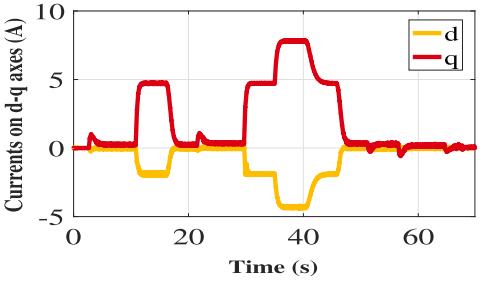

(d) i_{dq} currents

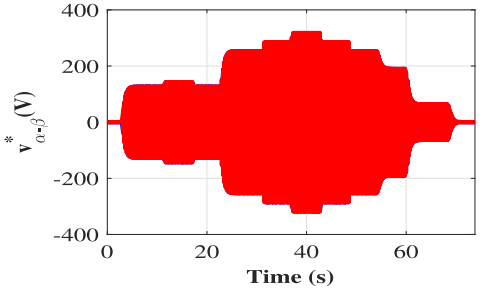

(e) Voltages in the α-β frame

FIGURE 11. Experimental results: proposed MTPA method at random speed/torque for 10HP IPMSM.

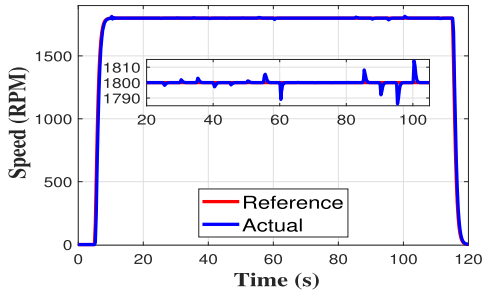

(a) Speed tracking

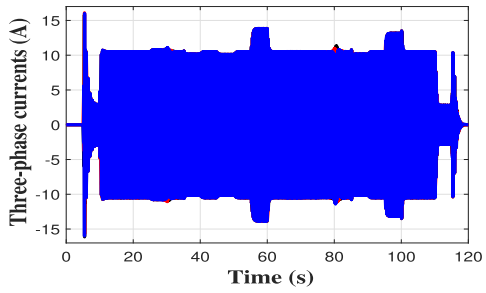

(b) Three-phase currents

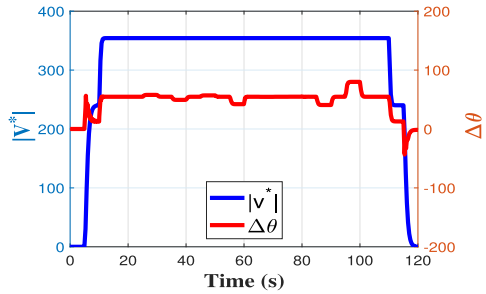

(c) Magnitude and angle of applied voltage

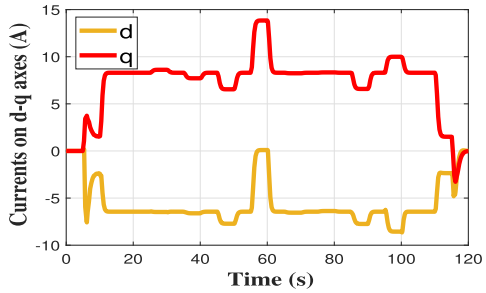

(d) i_{dq} currents

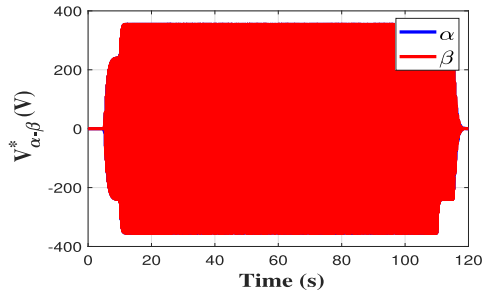

(e) Voltages in the α-β reference frame

FIGURE 12. Simulation result: proposed MTPA under machine's parameters variation for 10HP IPMSM.

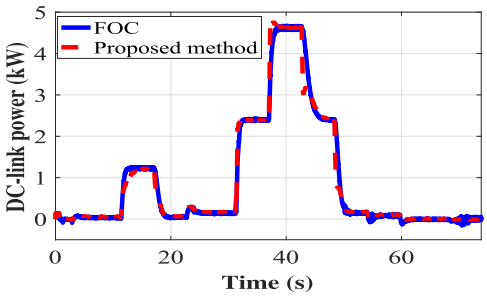

FIGURE 13. Comparison of DC-bus power.

TABLE 4. Performance index assessment for 10HP IPMSM.

	Proposed method	MTPA FOC
η_{dc}	$1.74 \cdot 10^5$ (97%)	$1.69 \cdot 10^5$ (100%)

The sensitivity function S_f^p is the ratio of a relative change in a function f to a relative change in a system parameter p. Accordingly, the sensitivity analysis is conducted at parameters L_d, L_q, R_s, and λ changing by $\pm 20\%$ in Table 3.

Besides, to assess the proposed MTPA controller versus the well-known vector control, the DC-bus power is considered as a criterion. The DC-bus power of both methods is shown in Fig. 13. The result reveals that the suggested MTPA method has a very similar power consumption as FOC. Furthermore, a performance index η_{dc} that calculates the DC-bus current integral during an experiment is introduced to quantify the efficiency performance numerically, i.e., $\eta_{dc} = \int_{t_0}^{t_f} I_{dc}\, dt$. The numerical results are shown in Table 4. The proposed MTPA control strategy yields 97% efficiency in the random speed and torque experiments. Therefore, the proposed MTPA control scheme is able to achieve MTPA operation without the need for current regulation.

VI. CONCLUSION

This manuscript presents a simple MTPA speed control method for IPMSM drives. This strategy eliminates the need for the motor's current regulation loop, making the control process much simpler. Acceptable dynamics in the presence of changing operating conditions are ensured by direct voltage control. As such, the torque angle is provided by a PI controller, and torque and speed compensation gains are then introduced to constrain the motor characteristics such that they provide a means to regulate the speed of the IPMSM by following the MTPA operation point. This control structure is simple when compared to conventional control strategies such as FOC while achieving comparable speed regulation performance and current consumption. Its effectiveness is also inspected experimentally and assessed versus the popular MTPA field-oriented control, which reaches 97%. Results reveal a high efficiency without the need for current control, which reduces complexity with respect to

conventional methods. The proposed control scheme achieves accurate MTPA trajectory tracking based on steady-state equations and does not consider high current/parameters error. Further, the robustness of the proposed control method's performance is confirmed against the machine's parameter variation. Nonetheless, good transient behavior is observed under numerous unpredictable load torque disturbances. The proposed MTPA controller is suitable for the development of low-cost motor drives and electric vehicle use. At the same time, the proposed method has the limitation of driving motors with high inertia mechanical loads, such as in trucks and oversize electrical vehicles. Therefore, it can be a good solution for personal EVs. Future work will consider transients to ensure optimal MTPA tracking at all operating conditions and system stability analysis, as well as THD analysis.

REFERENCES

[1] A. T. Nguyen, B. A. Basit, H. H. Choi, and J.-W. Jung, "Disturbance attenuation for surface-mounted PMSM drives using nonlinear disturbance observer-based sliding mode control," *IEEE Access*, vol. 8, pp. 86345–86356, 2020.

[2] X. Lin, W. Huang, W. Jiang, Y. Zhao, and S. Zhu, "Deadbeat direct torque and flux control for permanent magnet synchronous motor based on stator flux oriented," *IEEE Trans. Power Electron.*, vol. 35, no. 5, pp. 5078–5092, May 2020.

[3] C. Lascu and G.-D. Andreescu, "PLL position and speed observer with integrated current observer for sensorless PMSM drives," *IEEE Trans. Ind. Electron.*, vol. 67, no. 7, pp. 5990–5999, Jul. 2020.

[4] F. J. Anayi and M. M. A. Al Ibraheemi, "Estimation of rotor position for permanent magnet synchronous motor at standstill using sensorless voltage control scheme," *IEEE/ASME Trans. Mechatronics*, vol. 25, no. 3, pp. 1612–1621, Jun. 2020.

[5] K. Li and Y. Wang, "Maximum torque per ampere (MTPA) control for IPMSM drives using signal injection and an MTPA control law," *IEEE Trans. Ind. Informat.*, vol. 15, no. 10, pp. 5588–5598, Oct. 2019.

[6] Y. Zbede and J. Apsley, "Field weakening control of a PM vehicle drive," *J. Eng.*, vol. 2019, no. 17, pp. 3510–3515, Apr. 2019.

[7] S. Brock, D. Luczak, K. Nowopolski, T. Pajchrowski, and K. Zawirski, "Two approaches to speed control for multi-mass system with variable mechanical parameters," *IEEE Trans. Ind. Electron.*, vol. 64, no. 4, pp. 3338–3347, Apr. 2017.

[8] F. F. M. El-Sousy and K. A. Abuhasel, "Nonlinear robust optimal control via adaptive dynamic programming of permanent-magnet linear synchronous motor drive for uncertain two-axis motion control system," *IEEE Trans. Ind. Appl.*, vol. 56, no. 2, pp. 1940–1952, Mar. 2020.

[9] W. Liu, S. Chen, and H. Huang, "Adaptive nonsingular fast terminal sliding mode control for permanent magnet synchronous motor based on disturbance observer," *IEEE Access*, vol. 7, pp. 153791–153798, 2019.

[10] M. Liu, K. W. Chan, J. Hu, W. Xu, and J. Rodriguez, "Model predictive direct speed control with torque oscillation reduction for PMSM drives," *IEEE Trans. Ind. Informat.*, vol. 15, no. 9, pp. 4944–4956, Sep. 2019.

[11] P. Kou, D. Liang, J. Li, L. Gao, and Q. Ze, "Finite-control-set model predictive control for DFIG wind turbines," *IEEE Trans. Autom. Sci. Eng.*, vol. 15, no. 3, pp. 1004–1013, Jul. 2018.

[12] X. Liu and X. Kong, "Nonlinear model predictive control for DFIG-based wind power generation," *IEEE Trans. Autom. Sci. Eng.*, vol. 11, no. 4, pp. 1046–1055, Oct. 2014.

[13] Y. Han, C. Gong, L. Yan, H. Wen, Y. Wang, and K. Shen, "Multiobjective finite control set model predictive control using novel delay compensation technique for PMSM," *IEEE Trans. Power Electron.*, vol. 35, no. 10, pp. 11193–11204, Oct. 2020.

[14] T. Liu, A. Chen, C. Qin, J. Chen, and X. Li, "Double vector model predictive control to reduce common-mode voltage without weighting factors for three-level inverters," *IEEE Trans. Ind. Electron.*, vol. 67, no. 10, pp. 8980–8990, Oct. 2020.

[15] J. Ji, R. Xue, W. Zhao, T. Tao, and L. Huang, "Simplified three-vector-based model predictive thrust force control with cascaded optimization process for a double-side linear Vernier permanent magnet motor," *IEEE Trans. Power Electron.*, vol. 35, no. 10, pp. 10681–10689, Oct. 2020.

[16] C.-K. Lin, T.-H. Liu, J.-T. Yu, L.-C. Fu, and C.-F. Hsiao, "Model-free predictive current control for interior permanent-magnet synchronous motor drives based on current difference detection technique," *IEEE Trans. Ind. Electron.*, vol. 61, no. 2, pp. 667–681, Feb. 2014.

[17] S. Walz and M. Liserre, "Hysteresis model predictive current control for PMSM with LC filter considering different error shapes," *IEEE Open J. Power Electron.*, vol. 1, pp. 190–197, 2020.

[18] S. Ye and X. Yao, "A modified flux sliding-mode observer for the sensorless control of PMSMs with online stator resistance and inductance estimation," *IEEE Trans. Power Electron.*, vol. 35, no. 8, pp. 8652–8662, Aug. 2020.

[19] C. Gong, Y. Hu, J. Gao, Y. Wang, and L. Yan, "An improved delay-suppressed sliding-mode observer for sensorless vector-controlled PMSM," *IEEE Trans. Ind. Electron.*, vol. 67, no. 7, pp. 5913–5923, Jul. 2020.

[20] H. Ahmed and D. Çelik, "Sliding mode based adaptive linear neuron proportional resonant control of Vienna rectifier for performance improvement of electric vehicle charging system," *J. Power Sources*, vol. 542, Sep. 2022, Art. no. 231788. [Online]. Available: https://www.sciencedirect.com/science/article/pii/S0378775322007789

[21] X. Liu, H. Yu, J. Yu, and L. Zhao, "Combined speed and current terminal sliding mode control with nonlinear disturbance observer for PMSM drive," *IEEE Access*, vol. 6, pp. 29594–29601, 2018.

[22] A. Apte, V. A. Joshi, H. Mehta, and R. Walambe, "Disturbance-observer-based sensorless control of PMSM using integral state feedback controller," *IEEE Trans. Power Electron.*, vol. 35, no. 6, pp. 6082–6090, Jun. 2020.

[23] C. Wang, Z. Q. Zhu, and H. Zhan, "Adaptive voltage feedback controllers on nonsalient permanent magnet synchronous machine," *IEEE Trans. Ind. Appl.*, vol. 56, no. 2, pp. 1529–1542, Mar. 2020.

[24] H. Jie, G. Zheng, J. Zou, X. Xin, and L. Guo, "Adaptive decoupling control using radial basis function neural network for permanent magnet synchronous motor considering uncertain and time-varying parameters," *IEEE Access*, vol. 8, pp. 112323–112332, 2020.

[25] P. Gao, G. Zhang, H. Ouyang, and L. Mei, "An adaptive super twisting nonlinear fractional order PID sliding mode control of permanent magnet synchronous motor speed regulation system based on extended state observer," *IEEE Access*, vol. 8, pp. 53498–53510, 2020.

[26] K. A. Abuhasel, F. F. M. El-Sousy, M. F. El-Naggar, and A. Abu-Siada, "Adaptive RCMAC neural network dynamic surface control for permanent-magnet synchronous motors driven two-axis X-Y table," *IEEE Access*, vol. 7, pp. 38068–38084, 2019.

[27] S. Lu and X. Wang, "Command filtering-based neural network control for fractional-order PMSM with input saturation," *IEEE Access*, vol. 7, pp. 137811–137822, 2019.

[28] S. Li, H. Won, X. Fu, M. Fairbank, D. C. Wunsch, and E. Alonso, "Neural-network vector controller for permanent-magnet synchronous motor drives: Simulated and hardware-validated results," *IEEE Trans. Cybern.*, vol. 50, no. 7, pp. 3218–3230, Jul. 2020.

[29] H. Chaoui, M. Khayamy, and A. A. Aljarboua, "Adaptive interval type-2 fuzzy logic control for PMSM drives with a modified reference frame," *IEEE Trans. Ind. Electron.*, vol. 64, no. 5, pp. 3786–3797, May 2017.

[30] K. Li and Y. Wang, "Maximum torque per ampere (MTPA) control for IPMSM drives based on a variable-equivalent-parameter MTPA control law," *IEEE Trans. Power Electron.*, vol. 34, no. 7, pp. 7092–7102, Jul. 2019.

[31] Z. Han and J. Liu, "Comparative analysis of vibration and noise in IPMSM considering the effect of MTPA control algorithms for electric vehicles," *IEEE Trans. Power Electron.*, vol. 36, no. 6, pp. 6850–6862, Jun. 2021.

[32] T. Sun, M. Koç, and J. Wang, "MTPA control of IPMSM drives based on virtual signal injection considering machine parameter variations," *IEEE Trans. Ind. Electron.*, vol. 65, no. 8, pp. 6089–6098, Aug. 2018.

[33] Z. Chen, Y. Yan, T. Shi, X. Gu, Z. Wang, and C. Xia, "An accurate virtual signal injection control for IPMSM with improved torque output and widen speed region," *IEEE Trans. Power Electron.*, vol. 36, no. 2, pp. 1941–1953, Feb. 2021.

[34] K. Lee and Y. Han, "MTPA control strategy based on signal injection for V/f scalar-controlled surface permanent magnet synchronous machine drives," *IEEE Access*, vol. 8, pp. 96036–96044, 2020.

[35] D. Çelik and H. Ahmed, "Enhanced control of superconducting magnetic energy storage integrated UPQC for power quality improvement in EV charging station," *J. Energy Storage*, vol. 62, Jun. 2023, Art. no. 106843. [Online]. Available: https://www.sciencedirect.com/science/article/pii/S2352152X23002402

[36] T. Sun, J. Wang, C. Jia, and L. Peng, "Integration of FOC with DFVC for interior permanent magnet synchronous machine drives," *IEEE Access*, vol. 8, pp. 97935–97945, 2020.

[37] P. D. C. Perera, F. Blaabjerg, J. K. Pedersen, and P. Thogersen, "A sensorless, stable V/f control method for permanent-magnet synchronous motor drives," *IEEE Trans. Ind. Appl.*, vol. 39, no. 3, pp. 783–791, May/Jun. 2003.

[38] Z. Tang, X. Li, S. Dusmez, and B. Akin, "A new V/f-based sensorless MTPA control for IPMSM drives," *IEEE Trans. Power Electronics.*, vol. 31, no. 6, pp. 4400–4415, Jun. 2016.

[39] A. Ahmed, Y. Sozer, and M. Hamdan, "Maximum torque per ampere control for buried magnet PMSM based on DC-link power measurement," *IEEE Trans. Power Electron.*, vol. 32, no. 2, pp. 1299–1311, Feb. 2017.

[40] H. Chaoui and P. Sicard, "Adaptive fuzzy logic control of permanent magnet synchronous machines with nonlinear friction," *IEEE Trans. Ind. Electron.*, vol. 59, no. 2, pp. 1123–1133, Feb. 2012.

[41] J.-J. Chen and K.-P. Chin, "Automatic flux-weakening control of permanent magnet synchronous motors using a reduced-order controller," *IEEE Trans. Power Electron.*, vol. 15, no. 5, pp. 881–890, Sep. 2000.

[42] M. Khayamy and H. Chaoui, "Current sensorless MTPA operation of interior PMSM drives for vehicular applications," *IEEE Trans. Veh. Technol.*, vol. 67, no. 8, pp. 6872–6881, Aug. 2018.

[43] H. Chaoui, O. Okoye, and M. Khayamy, "Current sensorless MTPA for IPMSM drives," *IEEE/ASME Trans. Mechatronics*, vol. 22, no. 4, pp. 1585–1593, Aug. 2017.

[44] H. Chaoui, M. Khayamy, O. Okoye, and H. Gualous, "Simplified speed control of permanent magnet synchronous motors using genetic algorithms," *IEEE Trans. Power Electron.*, vol. 34, no. 4, pp. 3563–3574, Apr. 2019.

[45] M. Alzayed, "Simplified maximum torque per ampere trajectory tracking for permanent magnet synchronous machine drives," Ph.D. dissertation, Dept. Electron., Carleton Univ., Ottawa, ON, Canada, 2022, doi: 10.22215/etd/2022-15123.

[46] C. T. Krasopoulos, M. E. Beniakar, and A. G. Kladas, "Velocity and torque limit profile optimization of electric vehicle including limited overload," *IEEE Trans. Ind. Appl.*, vol. 53, no. 4, pp. 3907–3916, Jul./Aug. 2017.

[47] R. Al-Shehari, H. Chaoui, and H. Gualous, "MTPA trajectory tracking for IPMSM drives: A comparative study and analysis," in *Proc. IEEE Vehicle Power Propuls. Conf. (VPPC)*, Aug. 2018, pp. 1–6.

[48] M. Plesha, G. Gray, and F. Costanzo, *Engineering Mechanics: Statics and Dynamics*, 2nd ed. New York, NY, USA: McGraw-Hill, 2012, pp. 12–15.

[49] Z. Sun and G. G. Zhu, "Introduction of the automotive propulsion system," in *Design and Control of Automotive Propulsion Systems*. Boca Raton, FL, USA: Taylor & Francis, 2015, pp. 1–11.

[50] S. Bolognani, L. Peretti, and M. Zigliotto, "Parameter sensitivity analysis of an improved open-loop speed estimate for induction motor drives," *IEEE Trans. Power Electron.*, vol. 23, no. 4, pp. 2127–2135, Jul. 2008.

MOHAMAD ALZAYED (Member, IEEE) received the Ph.D. degree in electrical and computer engineering from Carleton University, Ottawa, ON, Canada. His career has bridged both academia and industry with more than 14 years of experience in control and electrical energy resources, grid management and efficiency, electrical design and contracting, and project management. Since 2019, he has been a member of the Intelligent Robotic and Energy Systems (IRES) Research Group, Department of Electronics, Carleton University. His teaching/research interests include intelligent control of electric machines and power converters for energy systems, real-time simulations, and power systems. He is a guest editor of several journals.

HICHAM CHAOUI (Senior Member, IEEE) received the Ph.D. degree in electrical engineering from the University of Quebec, Trois-Rivières, QC, Canada, in 2011. His career has spanned both academia and industry in the field of control and energy systems. From 2007 to 2014, he has held various engineering and management positions with Canadian industry. He is currently an Associate Professor with Texas Tech University, TX, USA, and also with Carleton University, Ottawa, ON, Canada. His scholarly work has resulted in more than 180 journals and conference publications. He was a recipient of the Best Thesis Award, the Governor General of Canada Gold Medal Award, the Carleton's Research Excellence Award, the Early Researcher Award from the Ministry of Colleges and Universities, and the Top Editor Recognition from IEEE Vehicular Technology Society. He is a Registered Professional Engineer in the province of Ontario and an associate editor of several IEEE journals.